Supplementary Materials

Evaluation of the halogenation and photofate of the blood pressure regulator losartan in water: Reactivity and mechanisms

Linke Jiang[a], Yong Li[b], Shuiqin Shi[a], Junmei Yan[a], Lianbao Chi[c,*],

Hui Liu[d], Mingbao Feng[a*]

[a] *Fujian Key Laboratory of Coastal Pollution Prevention and Control, College of the Environment & Ecology, Xiamen University, Xiamen 361102, China*

[b] *Guangzhou Hexin Instrument Co., Ltd., Guangzhou 510530, China*

[c] *CAS Key Laboratory of Marine Ecology and Environmental Sciences, Institute of Oceanology, Chinese Academy of Sciences, Qingdao 266071, China*

[d] *College of Biological, Chemical Sciences and Engineering, Jiaxing University, Zhejiang, Jiaxing 314001, China*

* Corresponding authors: Lianbao Chi

Email addresses: chilianbao@qdio.ac.cn

Mingbao Feng

Email address: mfeng24@xmu.edu.cn

Text S1. The kinetic analysis of reactions of LOS with the oxidant

The main equations used in the calculation are shown in Eqs. S1-S7.

$$\mathrm{HXO} \overset{K_{\mathrm{a,\,HXO}}}{\Longleftrightarrow} \mathrm{H^+} + \mathrm{XO^-},\ \mathrm{p}K_{\mathrm{a,\,HClO}} = 7.54,\ \mathrm{p}K_{\mathrm{a,\,HBrO}} = 8.62 \quad \text{(S1)}$$

$$\mathrm{LOS} \overset{K_{\mathrm{a,\,LOS}}}{\Longleftrightarrow} \mathrm{H^+} + \mathrm{LOS^-},\ \mathrm{p}K_{\mathrm{a,\,LOS}} = 4.26 \quad \text{(S2)}$$

$$\mathrm{LOS} + \mathrm{HXO} \overset{k_1}{\Rightarrow} \text{products} \quad \text{(S3)}$$

$$\mathrm{LOS} + \mathrm{XO^-} \overset{k_2}{\Rightarrow} \text{products} \quad \text{(S4)}$$

$$\mathrm{LOS^-} + \mathrm{HXO} \overset{k_3}{\Rightarrow} \text{products} \quad \text{(S5)}$$

$$\mathrm{LOS^-} + \mathrm{XO^-} \overset{k_4}{\Rightarrow} \text{products} \quad \text{(S6)}$$

$$k_{\mathrm{app,\,HXO}}\,[\mathrm{HXO}][\mathrm{LOS}]_{\mathrm{T}} = \sum_{\mathrm{i}=1,2} \alpha_i \beta_i [\mathrm{HXO}][\mathrm{LOS}]_{\mathrm{T}} \quad \text{(S7)}$$

The calculated results at pH 5.0 to 8.0 were listed as follows:

pH 5.0, $k_{\mathrm{app,\,HClO}} = 8.30\ \mathrm{M^{-1}\,s^{-1}}$, $k_{\mathrm{app,\,HBrO}} = 1.45\times10^{4}\ \mathrm{M^{-1}\,s^{-1}}$;

pH 6.0, $k_{\mathrm{app,\,HClO}} = 3.56\ \mathrm{M^{-1}\,s^{-1}}$, $k_{\mathrm{app,\,HBrO}} = 8.38\times10^{3}\ \mathrm{M^{-1}\,s^{-1}}$;

pH 7.0, $k_{\mathrm{app,\,HClO}} = 1.24\ \mathrm{M^{-1}\,s^{-1}}$, $k_{\mathrm{app,\,HBrO}} = 6.68\times10^{4}\ \mathrm{M^{-1}\,s^{-1}}$;

pH 8.0, $k_{\mathrm{app,\,HClO}} = 0.47\ \mathrm{M^{-1}\,s^{-1}}$, $k_{\mathrm{app,\,HBrO}} = 1.55\times10^{5}\ \mathrm{M^{-1}\,s^{-1}}$.

Text S2. The photodegradation experiments and calculation procedures

The experiments were categorized into direct and indirect photolysis sections to systematically assess photodegradation.

Direct photolysis. LOS solution (5.0 μM) was irradiated in a sunlight simulator at pH 7.0 and the first-order rate constant (k_{LOS}) was calculated as 9.89×10^{-7} s^{-1}. To reduce the instrument error, p-nitrophenyl (PNA)/pyridine photometry was selected and the photon fluence rate, $E_p°$ can be obtained by Eq. S8 [1].

$$E_p^\circ = \frac{k_{PNA}}{2.303\ \Phi_{PNA} \sum_{\lambda=290\ nm}^{800\ nm} (f_{p,\lambda}\ \varepsilon_{PNA,\lambda})} \quad (S8)$$

The irradiance of the incident photon, as determined through the medium of *p*-nitroanisole (PNA) in conjunction with pyridine (Pyr), was quantified at 3.42×10^{-8} Einstein cm^{-2} s^{-1}. In the equation, k_{PNA} was measured at 2.05×10^{-5} s^{-1} (Fig. S3) and Φ_{PNA} was calculated by Φ_{PNA}= 0.00029 + 0.29[Pyr] [2]. According to Eq. S14, the direct photolysis quantum yield of LOS is Φ_{LOS} = 1.10×10^{-6}.

Reactivity with $^{\bullet}$OH. The experiment was conducted using the UV/H_2O_2 method [3] at pH 7.0, with NB (5.0 μM) as the probe compound. The pseudo-first-order rate constant of LOS can be evaluated by Eqs. S9 and S10:

$$[\bullet OH]_{SS} = \frac{k'_{NB} - k'_{NB,\,UV}}{k_{NB,\,\bullet OH}} \quad (S9)$$

$$k'_{LOS} = k'_{LOS,\,\bullet OH} \times [\bullet OH]_{SS} + k'_{LOS,\,UV} \quad (S10)$$

In which $k'_{NB,\,\bullet OH}$ was 3.90×10^{9} M^{-1} s^{-1} [3]; k'_{NB} measured at 5.90×10^{-5} M^{-1} s^{-1} means the pseudo-first-order rate constant obtained using UV/H_2O_2 method; according to the experiments, $k'_{NB,\,UV}$ was negligible; k'_{LOS} was the pseudo-first-order rate constant in UV/H_2O_2 treatment; $k'_{LOS,\,\bullet OH}$ was the pseudo-first-order rate constant in H_2O_2 treatment; $k'_{LOS,\,UV}$ was the radiation only with UV. The NB and LOS degradation by $^{\bullet}$OH were tested separately. The values of the constants are shown in Fig. S4, and by calculation, $k'_{LOS,\,\bullet OH}$ = 1.76×10^{7} M^{-1} s^{-1}.

Reactivity with $CO_3^{\bullet-}$. The system was conducted under the conditions of [$NaHCO_3$] = 0.1 M, [$NaNO_3$] = 10.0 mM, and [LOS] = 10.0 μM at pH 7.0, with L-Tyrosine (Tyr, 10.0 μM) chosen as the reference compound [4] to evaluate the reactivity with $CO_3^{\bullet-}$. The computed ratio of the

pseudo-first-order rate constants in LOS and Tyr systems was S = k_{LOS}/k_{Tyr} = 0.627, and $k_{LOS,\ CO_3^{\bullet-}}$ can be measured to be 2.89×10^7 M^{-1} s^{-1} by Eqs. S11-S13 shown in Fig. S5.

$$S = \frac{R_{^\bullet OH}^{LOS} + R_{CO_3^{\bullet-}}^{LOS}}{R_{^\bullet OH}^{Tyr} + R_{CO_3^{\bullet-}}^{Tyr}} \quad (S11)$$

$$R_{CO_3^{\bullet-}}^{LOS} = R_{CO_3^{\bullet-}} \frac{k_{LOS,\ CO_3^{\bullet-}}}{k_{Tyr,\ CO_3^{\bullet-}} + k_{LOS,\ CO_3^{\bullet-}}} \quad (S12)$$

$$R_{CO_3^{\bullet-}}^{Tyr} = R_{CO_3^{\bullet-}} \frac{k_{Tyr,\ CO_3^{\bullet-}}}{k_{Tyr,\ CO_3^{\bullet-}} + k_{LOS,\ CO_3^{\bullet-}}} \quad (S13)$$

Reactivity with $^1O_2$. The experiment involved using 5.0-20.0 μM LOS,10.0 μM Rose Bengal (RB) to create singlet oxygen ($^1O_2$) at pH 7.0, and 0.1 mM furfuryl alcohol (FFA) to measure the rate of $^1O_2$ (R_{1O2}) [5]. The calculation for $k_{LOS,\ 1O2}$ can be found in Fig. S6, which was computed to be 9.36×10^7 M^{-1} s^{-1} by Eq. S14 with $k_{1O2} = 2.50\times10^5$ s^{-1} as the decay rate constant of $^1O_2$ [6].

$$R_{LOS} = \frac{R_{1O_2}\, k_{LOS,1O_2}\, [LOS]}{k_{1O_2} + k_{LOS,1O_2}\, [LOS]} \quad (S14)$$

Reactivity with ^{3}AQ2S*. Fig. S7 shows the degradation rates of different concentrations of LOS at pH 7.0 with the addition of AQ2S to form ^{3}AQ2S*. From Fig. S7B, R_{LOS} = 6.40×10^{-5} [LOS] was estimated by the linear trend. The photodegradation rate of LOS by ^{3}AQ2S* was calculated as shown in Eq. S15 [5].

$$R_{LOS} = \Phi_{^3AQ2S^*} \times P_a^{AQ2S} \times \frac{k_{^3AQ2S^*,\ LOS} \times [LOS]}{k_{^3AQ2S^*} + k_{^3AQ2S^*,\ LOS} \times [LOS]} \quad (S15)$$

In the equation, $\Phi_{^3AQ2S^*}$ = 0.18 as the generation quantum yield; the photon flux P_a^{AQ2S} = 1.92×10^{-4} Einstein L^{-1} s^{-1}; and the deactivation rate constant $k_{^3AQ2S^*}$ = 1.1×10^7 s^{-1} [7]. Empirically, we can get $k_{^3AQ2S^*,\ LOS}$ [LOS] << $k_{^3AQ2S^*}$, so that the equation can change to $k_{^3AQ2S^*,\ LOS} = \frac{R_{LOS}\, k_{^3AQ2S^*}}{\Phi_{^3AQ2S^*} P_a^{AQ2S} [LOS]}$ and by the formula $k_{^3AQ2S^*,\ LOS}$ = 2.04×10^7 M^{-1} s^{-1} was calculated and $k_{^3AQ2S^*,\ LOS}$ [LOS] << $k_{^3AQ2S^*}$ can be confirmed.

Text S3. Analytical methods

The computer prediction tool APEX was used to forecast the photoinduced transformation kinetics of LOS in surface water by considering photoreactivity parameters and water depth [8]. The relationships between half-life and the fractions of LOS degradation at 0.5 m water depth and DOC (mg/L) can be predicted by APEX in SSD (summer sunny day).

HPLC was used to detect the signals of LOS and measure its degradation rates during the chlorination, bromination, and solar/chlorine experiments. Agilent C_{18} column (Zorbax Eclipse XDB, 5 μm, 4.6×150 mm) was used for chromatographical separation and determination of the target compounds. Details of the detection wavelength, mobile phase ratio (methanol and water), flow rate, and retention time are displayed in Table S1. LOS and TPs formed in the chlorination, bromination, and solar/chlorine systems were concentrated by solid-phase extraction (SPE) using Waters Oasis HLB cartridge (WAT106202, 6 cc/200 mg). Before SPE, 5 mL methanol and water were successively added to the HLB, and then 40 mL reaction samples were poured and dried for 20-30 min. Prior to LC-HRMS analysis, the cartridge was washed with 5 mL of methanol in order to extract the final reaction products. In addition, the chemical structures of different TPs generated during LOS degradation were identified using an AB Sciex Triple TOF 5600+ LC-HRMS. The electrospray ion source used positive and negative ion modes to detect different chemical components of TP molecules.

Text S4. The MS/MS fragments of LOS and its TPs

(1) LOS: The *m/z* value of the LOS molecule was 423.1695 in the ESI positive mode. Two MS/MS fragments (*m/z* 235.0978, *m/z* 207.0895) were detected, which could be ascribed to the losses of $C_8H_{12}ClN_2O$ or $C_{14}H_{10}N_4$ moieties from AML (Fig. S8A).

(2) TP-470: One fragment (*m/z* 243.0906) was discovered in the ESI negative mode for TP-470 (*m/z* 469.0549), which can be indicated as the loss of $C_{10}H_{11}BrN_4$ moiety plus the addition of six H atoms and hydroxyl group from TP-470 (Fig. S8B).

(3) TP-438: Four fragments (*m/z* 421.1358, *m/z* 235.0978, *m/z* 207.0895, *m/z* 205.0738) were discovered in the ESI positive mode for TP-438 (*m/z* 439.1644), which can be ascribed to the loss of hydroxyl group and the aldehyde formation from *m/z* 439.1644, together with further losses of $C_8H_{10}ClN_2O$ and $C_{14}H_{10}N_4O$ moieties, and the addition of two H atoms and hydroxyl group from *m/z* 421.1358, the aldehyde formation from *m/z* 207.0895 (Fig. S8C).

(4) TP-426: TP-426 (*m/z* 427.1199) had three MS/MS fragments (*m/z* 235.0978, *m/z* 207.0895, and *m/z* 205.0738), which could be ascribed to the losses of $C_7H_9Cl_2N_2$ or $C_{13}H_9N_4$ moieties, and the addition of two H atoms and hydroxyl group from TP-426, and the aldehyde formation from *m/z* 207.0895 (Fig. S8D).

(5) TP-420: The *m/z* value of TP-420 was 421.1538 in the ESI positive mode. Three MS/MS fragments (*m/z* 235.0978, *m/z* 207.0895, *m/z* 205.0738) were detected, which could be ascribed to the losses of $C_8H_{10}ClN_2O$ or $C_{14}H_{10}N_4O$ moieties together with the addition of two H atoms and hydroxyl group from TP-420 plus the aldehyde formation from *m/z* 207.0895 (Fig. S8E).

(6) TP-334: TP-334 (*m/z* 333.1833) had two MS/MS fragments (*m/z* 159.0676 and *m/z* 145.0520), which could be indicated as the loss of $C_{11}H_{14}N_2$ moiety from TP-334, together with the further loss of CH_2 from *m/z* 159.0676 (Fig. S8F).

(7) TP-252: The *m/z* value of TP-252 was 253.1084 in the ESI positive mode. One MS/MS fragment (*m/z* 207.0895) was detected, which could be ascribed to the loss of C_6N_2 moiety together with the addition of two H and Cl atoms plus hydroxyl group from TP-252 (Fig. S8G).

(8) TP-251: In the ESI positive mode, TP-251 (*m/z* 252.1244) had one characteristic MS/MS fragment as *m/z* 235.0978. It represented the loss of NH_2 from *m/z* 235.0978 (Fig. S8H).

(9) TP-238: TP-238 (*m/z* 239.0927) had three MS/MS fragments (*m/z* 97.0648, *m/z* 85.0648 and *m/z* 69.0335), which could be indicated as the loss of $C_7H_5N_4$ moiety and the addition of four H atoms from TP-238, together with the further loss of CH from *m/z* 97.0648 and the loss of CH_3 with the aldehyde formation from *m/z* 85.0648 (Fig. S8I).

(10) TP-206: The *m/z* value of TP-206 was 207.0895 in the ESI positive mode. One MS/MS fragment (*m/z* 205.0738) was detected, which could be ascribed to the aldehyde formation from *m/z* 207.0895 (Fig. S8J).

(11) TP-204: One fragment (*m/z* 71.0604) was discovered in the ESI positive mode for TP-204 (*m/z* 205.0738), which can be indicated as the loss of $C_5H_7ClO_2$ moiety from TP-204 (Fig. S8K).

(12) TP-188: TP-188 (*m/z* 187.0989) had one MS/MS fragment (*m/z* 97.0659), which could be indicated as the loss of $C_4H_8N_4$ moiety and the addition of five H atoms and hydroxyl group from TP-188 (Fig. S8L).

(13) TP-174: In the ESI negative mode, TP-174 (*m/z* 173.0833) had one characteristic MS/MS fragment as *m/z* 83.0502, which could be represented the loss of $C_4H_3N_4$ and the addition of hydroxyl group from *m/z* 173.0833 (Fig. S8M).

(14) TP-160: The *m/z* value of TP-160 was 159.0676 in the ESI negative mode. Three MS/MS fragments (*m/z* 97.0659, *m/z* 95.0502, *m/z* 69.0346) was detected, which could be ascribed to the loss of $C_2H_4N_4$ and the addition of five H atoms and hydroxyl group from *m/z* 159.0676, plus the further aldehyde formation from *m/z* 97.0659 and the loss of C_2H_2 from *m/z* 95.0502 (Fig. S8N).

(15) TP-146: One fragment (*m/z* 83.0502) was discovered in the ESI negative mode for TP-146 (*m/z* 145.0520), which can be indicated as the loss of $C_2H_2N_4$ moiety and the addition of three H atoms and hydroxyl group from TP-146 (Fig. S8O).

Table S1. HPLC conditions of the chemicals in this study.

Chemicals	Abbr.	Mobile phase Methanol/water	Flow rate (mL/min)	UV_{max} (nm)	Retention time (min)
Losartan	LOS	67:33	0.8	205	6.801
Methylparaben	MeP	60:40	0.8	256	3.695
Furfuryl alcohol	FFA	13:87	0.8	217	7.816
L-Tyrosine	Tyr	10:90	0.8	223	4.299
p-Nitroanisole	PNA	80:20	0.8	316	2.989
Nitrobenzene	NB	65:35	0.8	262	4.933

Table S2. The product information of LOS and its TPs, determined using a high-resolution LC-MS technique.

Comp.	Molecular formula	R_t (min)	ESI positive			ESI negative			Structure
			Measured *m/z*	Calculated *m/z*	Error (ppm)	Measured *m/z*	Calculated *m/z*	Error (ppm)	
LOS	$C_{22}H_{23}ClN_6O$	5.40	423.1701	423.1695	1.42				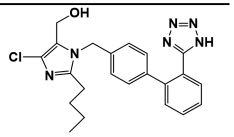
TP-470	$C_{21}H_{20}BrClN_6$	5.40				469.0547	469.0549	-0.43	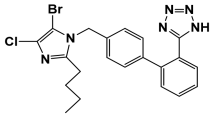
TP-438	$C_{22}H_{23}ClN_6O_2$	5.32	439.1637	439.1644	-1.59				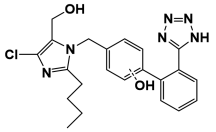
TP-426	$C_{21}H_{20}Cl_2N_6$	5.69	427.1206	427.1199	1.64	425.1049	425.1054	-1.18	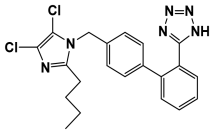
TP-420	$C_{22}H_{21}ClN_6O$	5.60	421.1538	421.1538	0	419.1398	419.1393	1.19	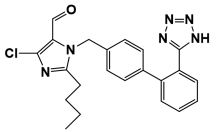
TP-334	$C_{19}H_{22}N_6$	5.02	335.1979	335.1979	0	333.1842	333.1833	2.70	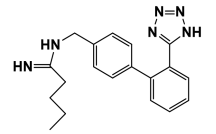

TP-252	$C_{14}H_{12}N_4O$	5.52				251.0936	251.0938	-0.80	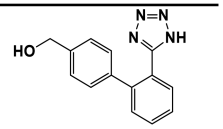
TP-251	$C_{14}H_{13}N_5$	4.92				250.1103	250.1098	2.00	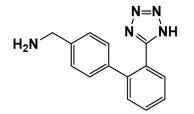
TP-238	$C_{13}H_{10}N_4O$	4.91	239.0899	239.0927	-11.71				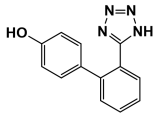
TP-206	$C_8H_{15}ClN_2O_2$	4.92	207.0912	207.0895	8.21				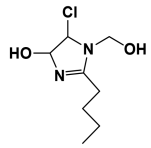
TP-204	$C_8H_{13}ClN_2O_2$	5.08	205.0760	205.0738	10.73				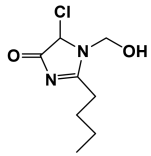
TP-188	$C_{10}H_{12}N_4$	5.26				187.0977	187.0989	-6.41	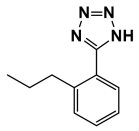
TP-174	$C_9H_{10}N_4$	5.18				173.0821	173.0833	-6.93	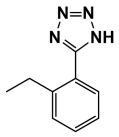

TP-160	$C_8H_8N_4$	5.10	159.0661	159.0672	-9.43	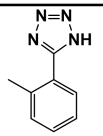
TP-146	$C_7H_6N_4$	4.97	145.0504	145.0520	-11.03	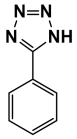

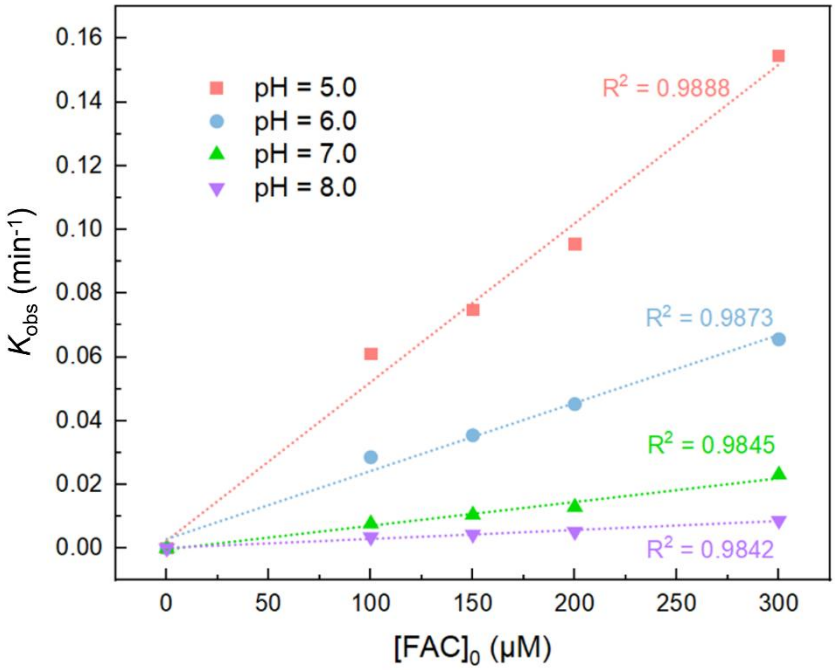

Fig. S1. The linear fitting observed between the measured pseudo-first-order rate constants ($k_{obs,\ LOS}$, s^{-1}) of LOS and FAC concentrations (0-300.0 μM).

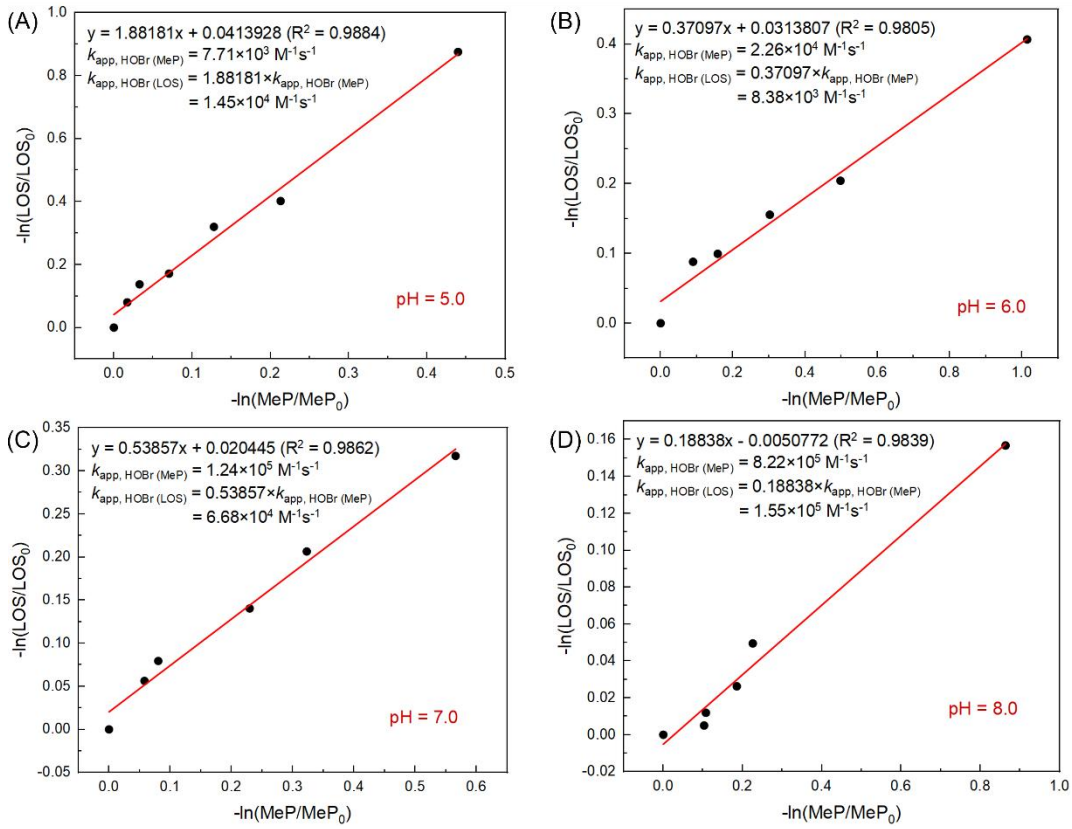

Fig. S2. Linear relationship between the second-order rate constants of LOS and MeP in bromination at (A) pH 5.0, (B) pH 6.0, (C) pH 7.0, (D) pH 8.0.

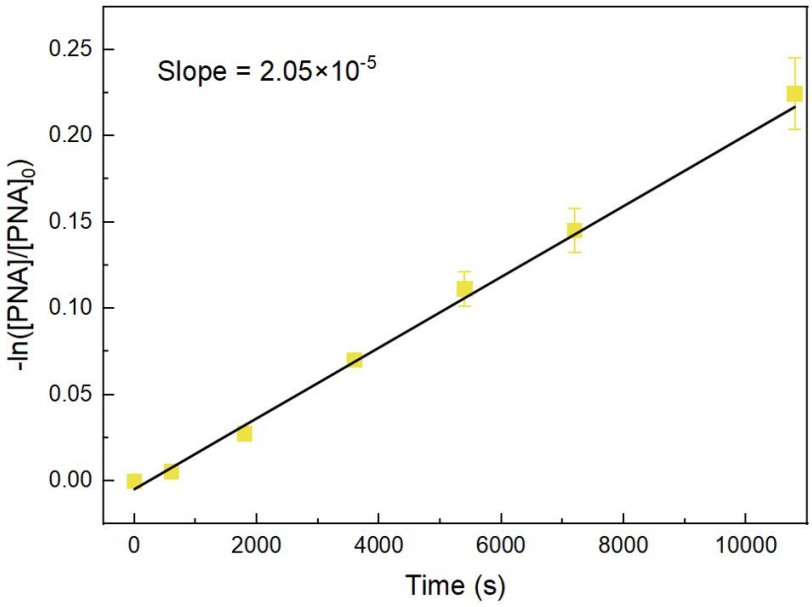

Fig. S3. Degradation of PNA (10.0 μM) in the solar simulator at pH 7.0. Conditions: xenon arc lamp intensity = 300 W/m^2, 10.0 mM pyridine.

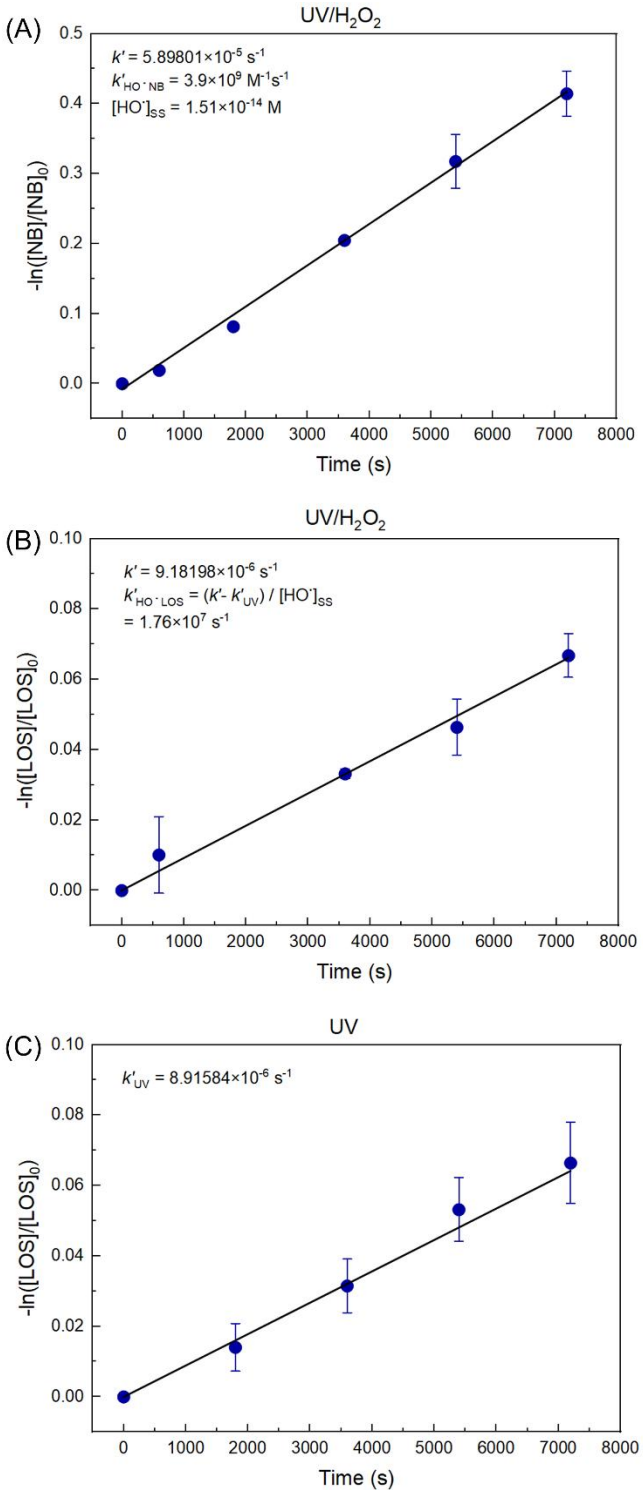

Fig. S4. The pseudo-first-order rate constants of (A) NB and (B) LOS by UV/H_2O_2 treatment; and measured pseudo-first-order rate constants of (C) LOS by UV treatment. Conditions: $[LOS]_0$ = 5.0 μM, $[Na_2HPO_4]_0$ = 10.0 mM, $[NB]_0$ = 5.0 μM, $[H_2O_2]_0$ = 50.0 μM, pH 7.0.

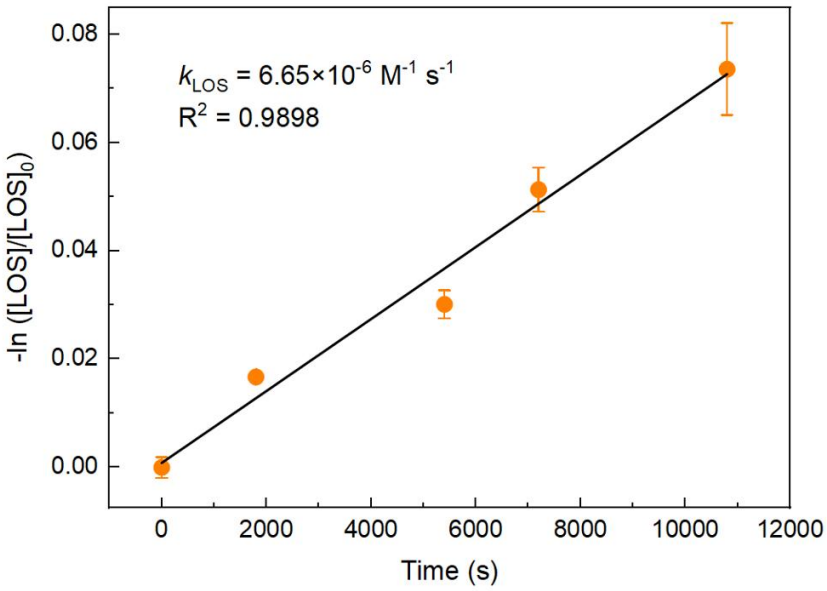

Fig. S5. Degradation of LOS by $CO_3^{\bullet-}$ in phosphate buffer solution. Conditions: xenon arc lamp intensity = 300 W/m^2, $[LOS]_0$ = 10.0 μM, $[Na_2HPO_4]_0$ = 10.0 mM, $[NaHCO_3]_0$ = 0.1 M, $[NaNO_3]_0$ = 10.0 mM, pH 7.0.

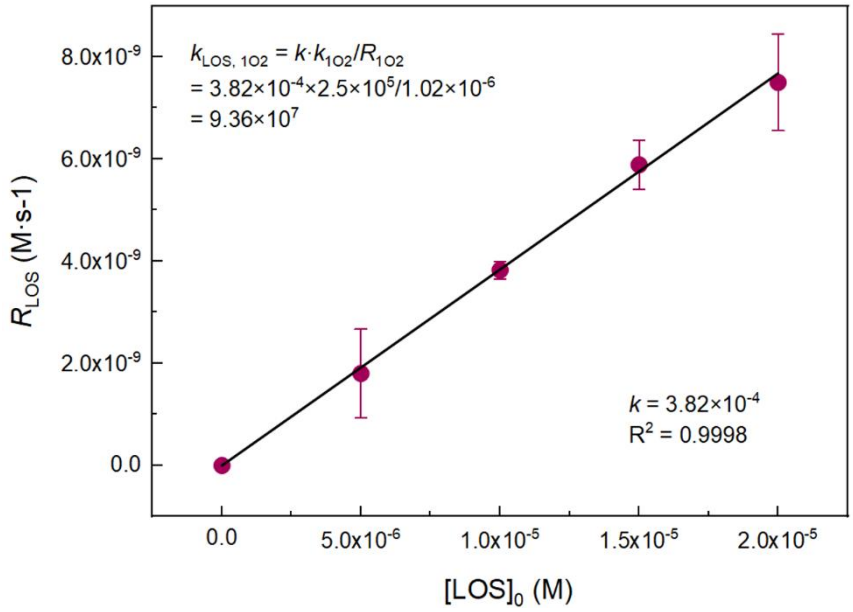

Fig. S6. Measured photodegradation rates of LOS under irradiation with RB as the $^1O_2$ source. Conditions: xenon arc lamp intensity = 300 W/m^2, $[LOS]_0$ = 10.0 μM, $[Na_2HPO_4]_0$ = 10.0 mM, $[RB]_0$ = 10.0 μM, pH 7.0.

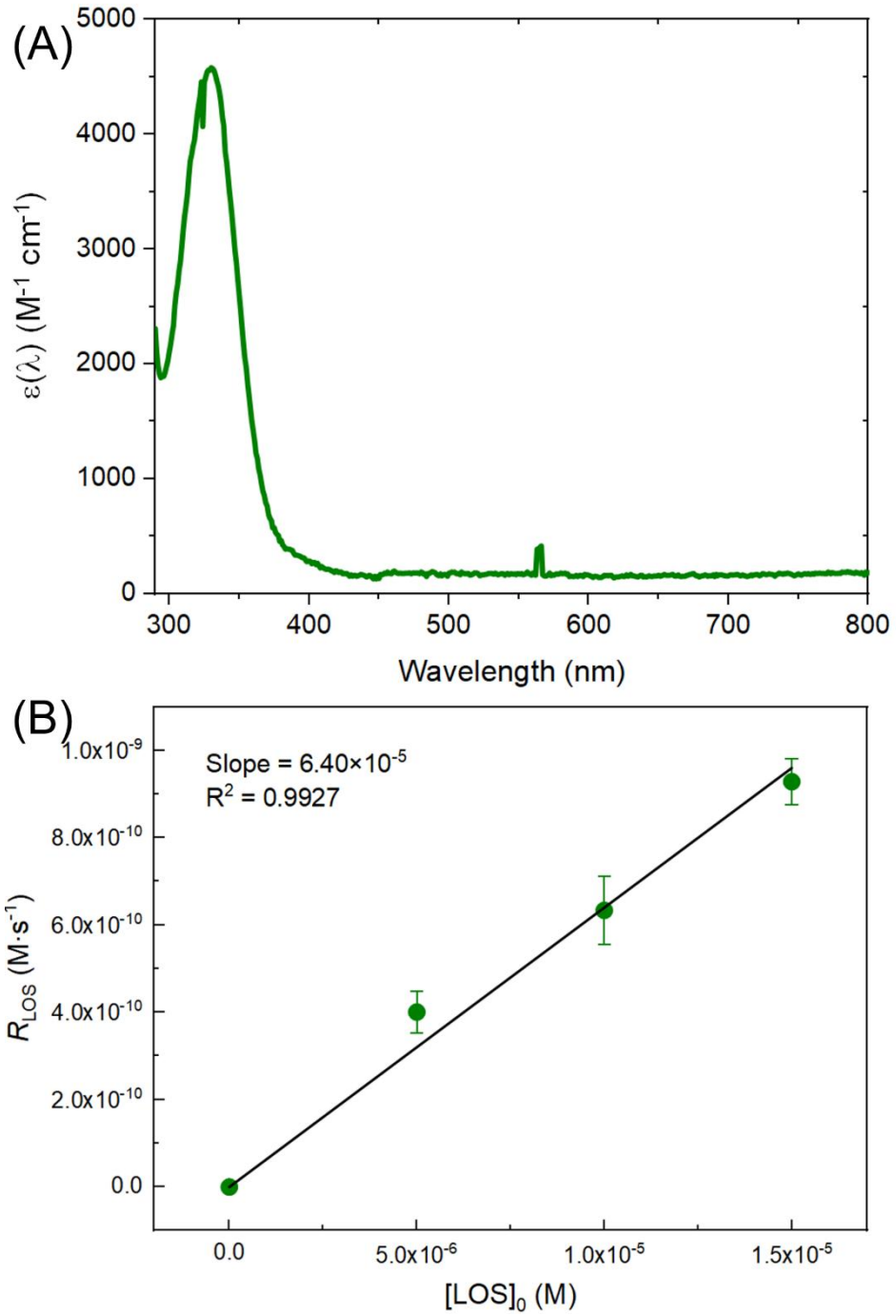

Fig. S7. (A) The spectral absorption characteristics of AQ2S and (B) the linear relationship between photodegradation rates of LOS reacted with 0.1 mM AQ2S and $[LOS]_0$ at pH 7.0.

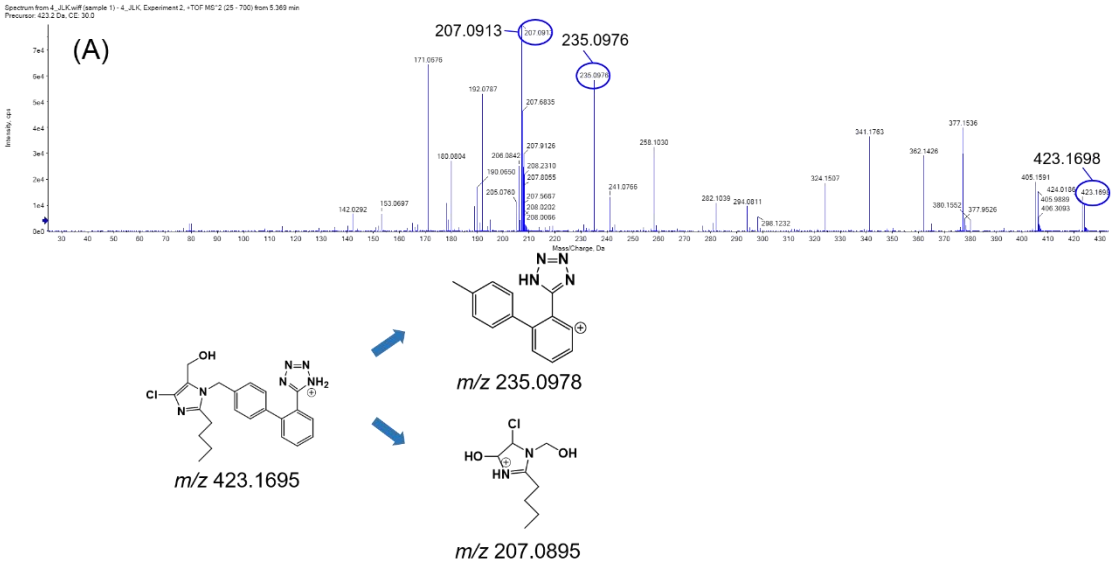
(A)
207.0913
235.0976
423.1698
m/z 423.1695
m/z 235.0978
m/z 207.0895

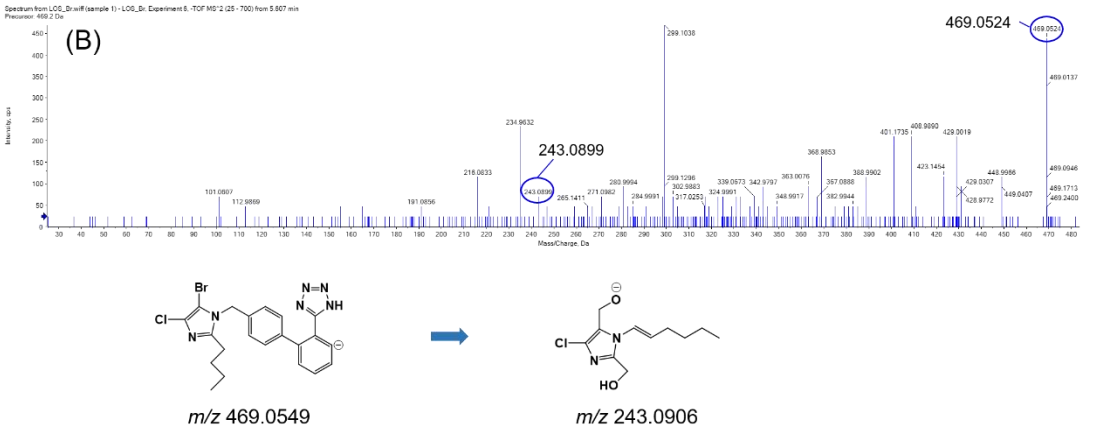
(B)
469.0524
243.0899
m/z 469.0549
m/z 243.0906

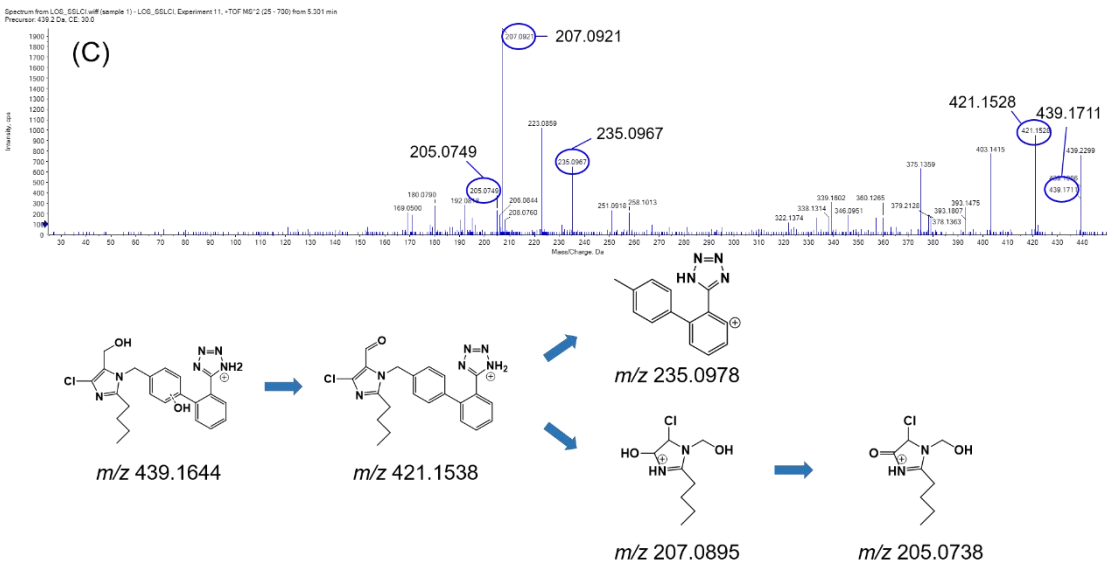
(C)
207.0921
421.1528
439.1711
235.0967
205.0749
m/z 439.1644
m/z 421.1538
m/z 235.0978
m/z 207.0895
m/z 205.0738

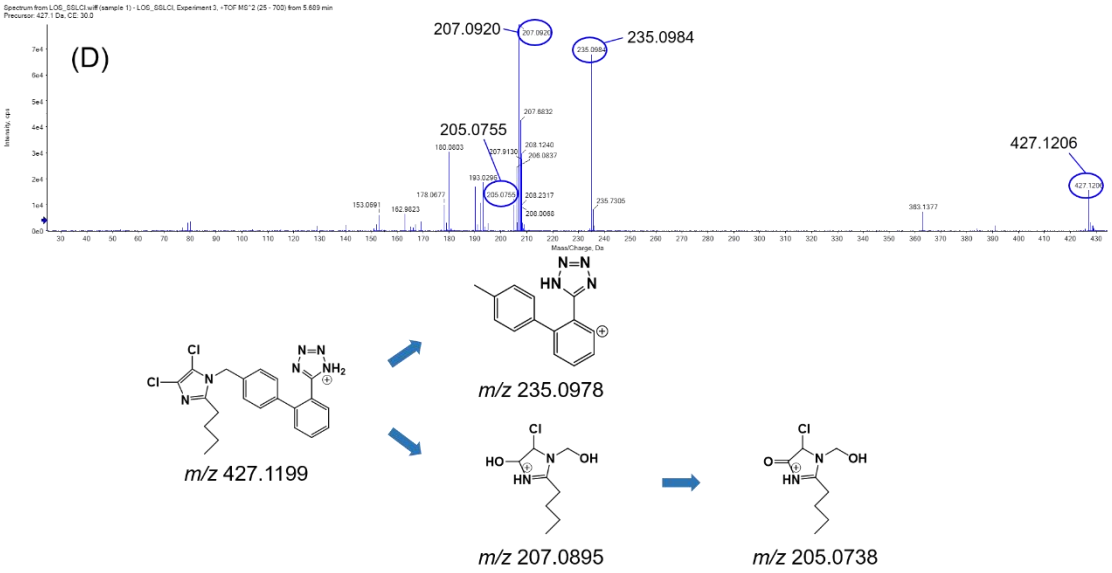
(D)
207.0920
235.0984
205.0755
427.1206
m/z 235.0978
m/z 427.1199
m/z 207.0895
m/z 205.0738

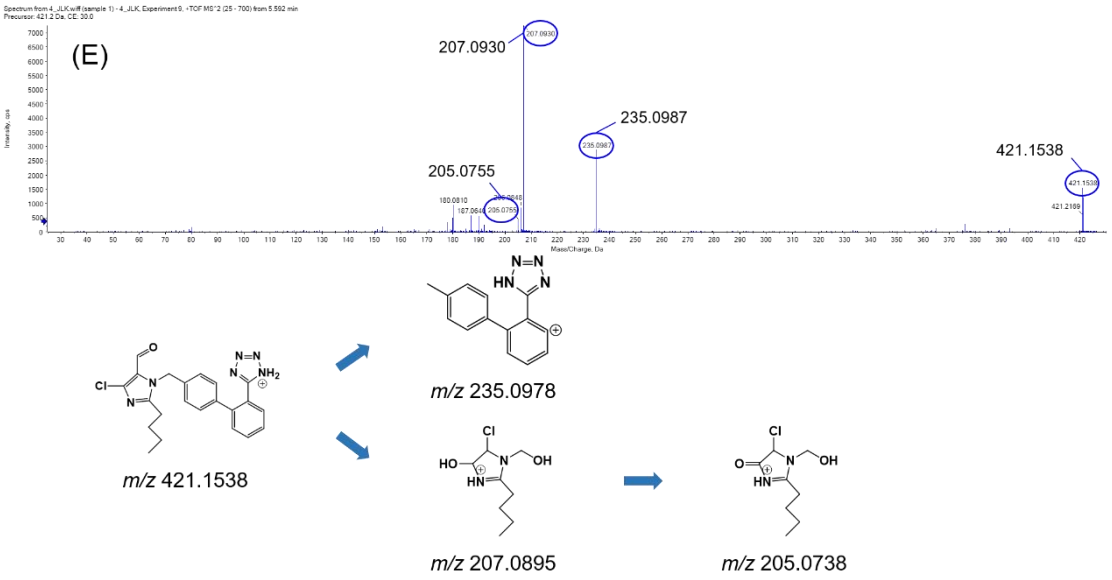
(E)
207.0930
235.0987
205.0755
421.1538
m/z 235.0978
m/z 421.1538
m/z 207.0895
m/z 205.0738

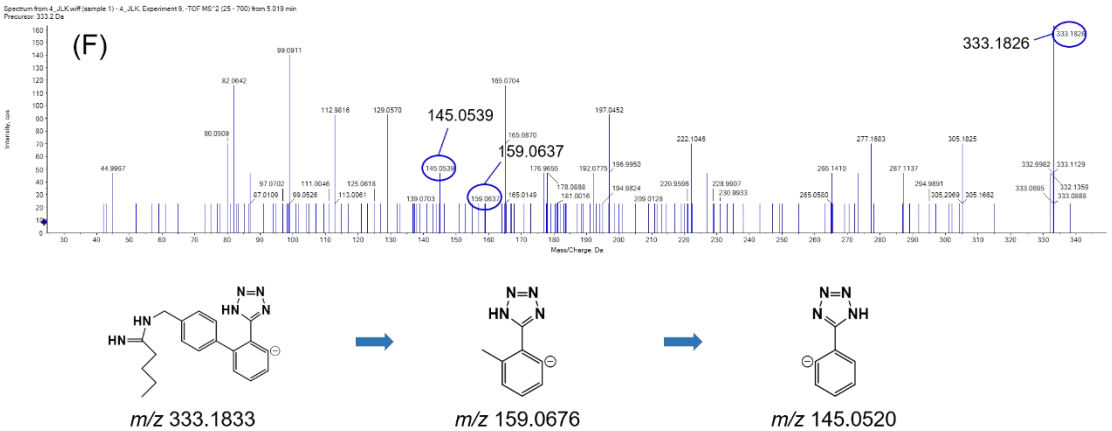
(F)
333.1826
145.0539
159.0637
m/z 333.1833
m/z 159.0676
m/z 145.0520

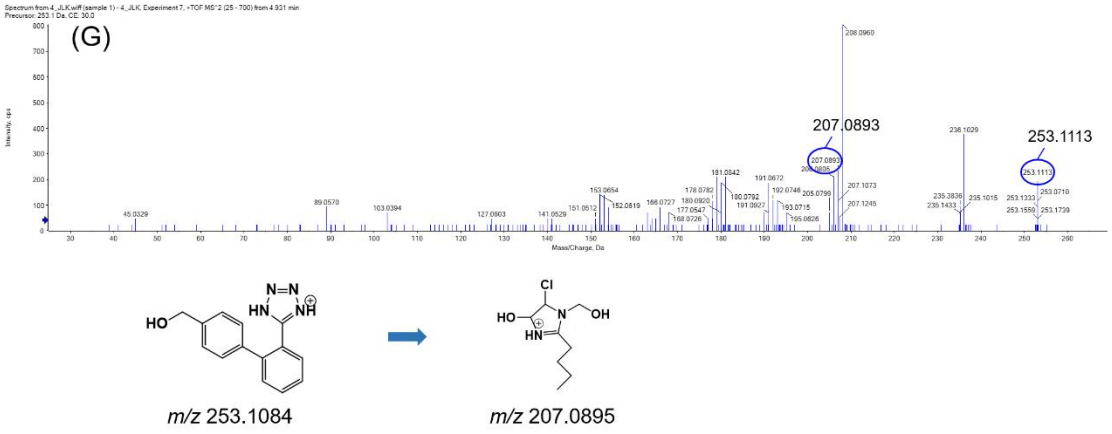
(G)
207.0893
253.1113
m/z 253.1084
m/z 207.0895

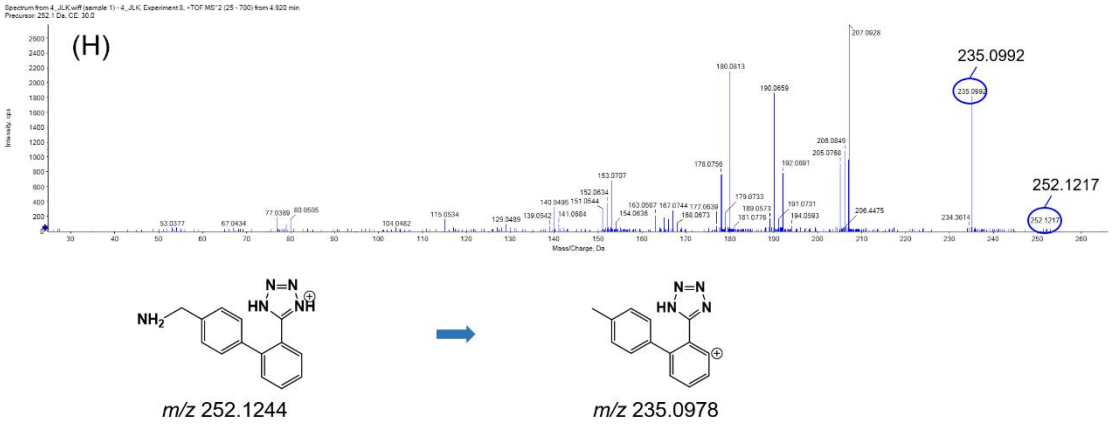
(H)
235.0992
252.1217
m/z 252.1244
m/z 235.0978

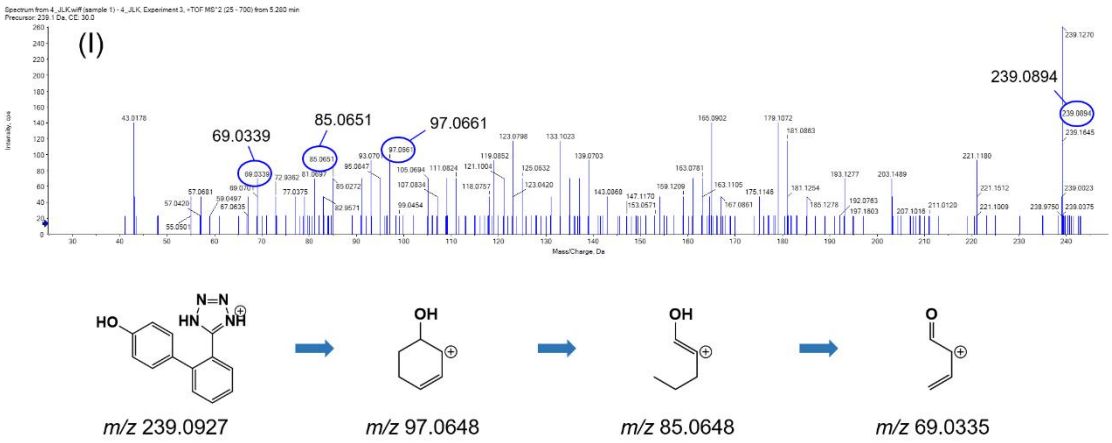
(I)
239.0894
69.0339
85.0651
97.0661
m/z 239.0927
m/z 97.0648
m/z 85.0648
m/z 69.0335

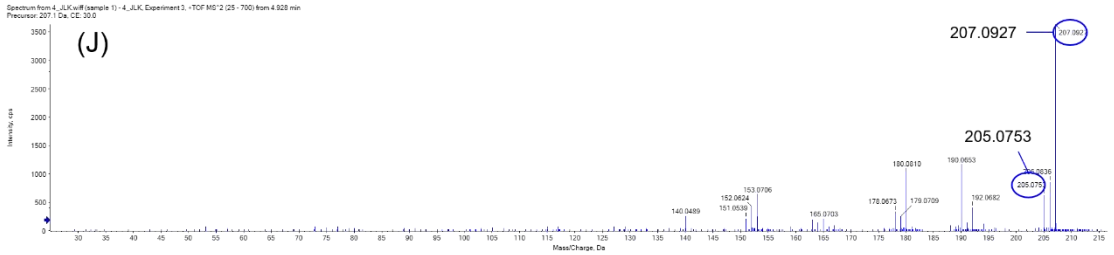

m/z 207.0895 *m/z* 205.0738

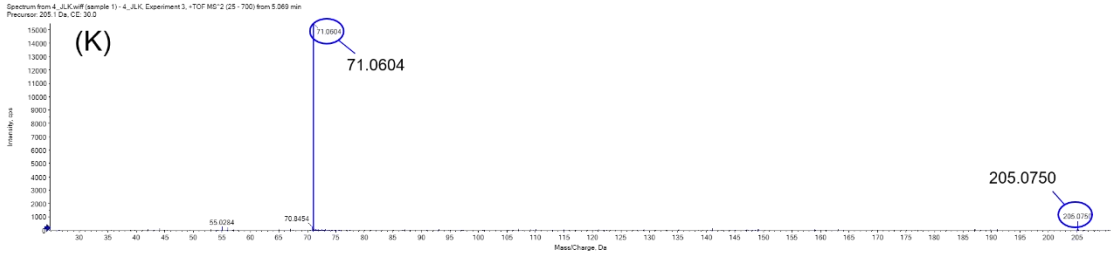

m/z 205.0738 *m/z* 71.0604

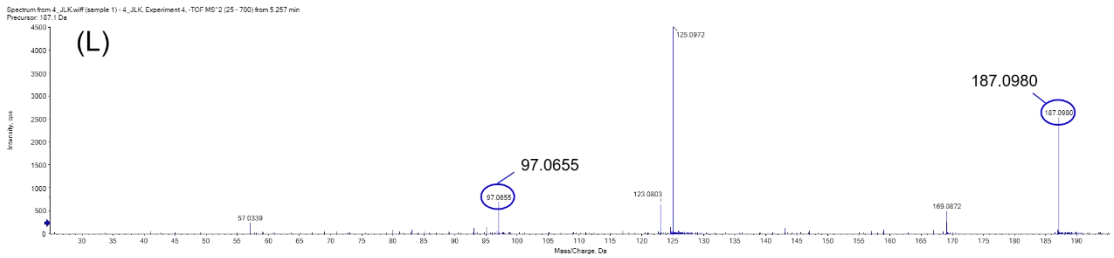

m/z 187.0989 *m/z* 97.0659

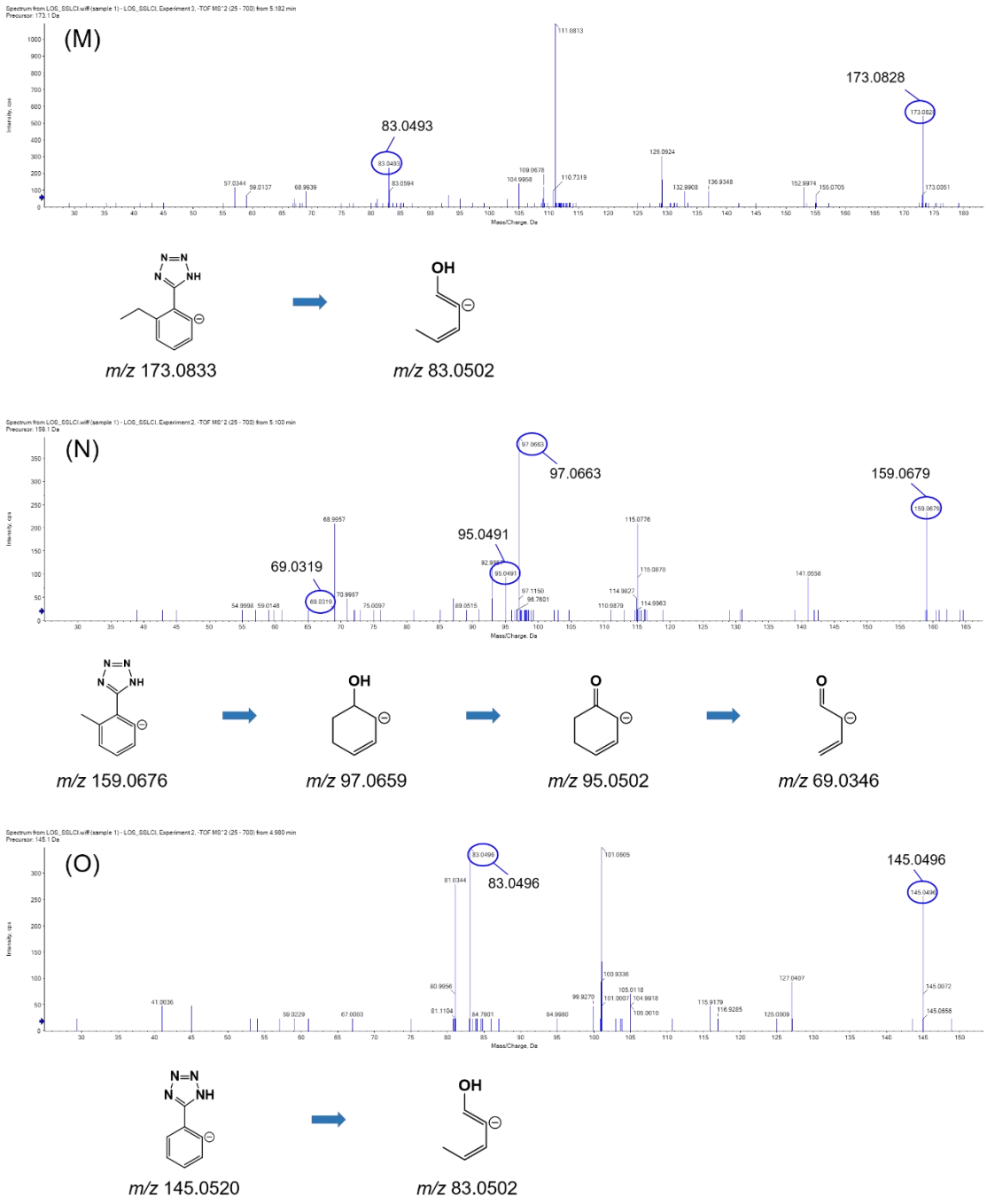

Fig. S8. The MS/MS spectra and the proposed fragmentation patterns of LOS and its TPs in chlorination, bromination and solar/chlorine systems at pH 7.0 in phosphate buffer solution. (A) LOS, (B) TP-470, (C) TP-438, (D) TP-426, (E) TP-420, (F) TP-334, (G) TP-252, (H) TP-251, (I) TP-238, (J) TP-206, (K) TP-204, (L) TP-188, (M) TP-174, (N) TP-160, (O) TP-146.

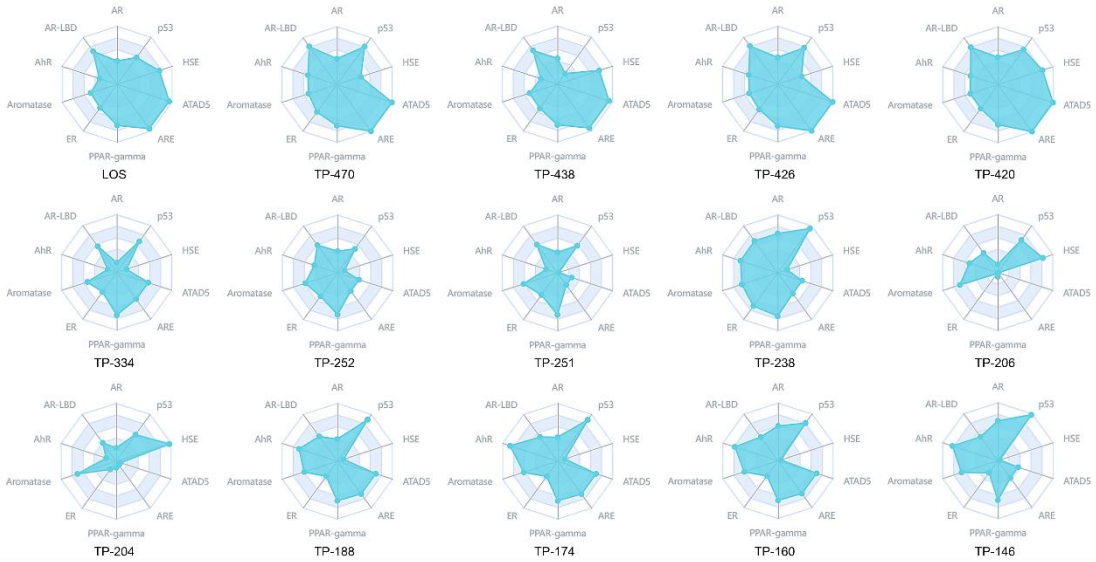

Fig. S9. The endocrine disruption prediction of LOS and its TPs based on EDC-Predictor.

Supplementary References

[1] S. Buckley, F. Leresche, B. Hanson, F.L. Rosario-Ortiz, 2023. Decoupling Optical Response and Photochemical Formation of Singlet Oxygen in Size Isolated Fractions of Ozonated Dissolved Organic Matter, Environ Sci Technol 57, 5603–5610.

[2] J.R. Laszakovits, S.M. Berg, B.G. Anderson, J.E. O'Brien, K.H. Wammer, C.M. Sharpless, 2017. P-Nitroanisole/pyridine and p-Nitroacetophenone/pyridine actinometers revisited: Quantum yield in comparison to ferrioxalate, Environ Sci Technol Lett 4, 11–14.

[3] M.J. Watts, K.G. Linden, 2007. Chlorine photolysis and subsequent OH radical production during UV treatment of chlorinated water, Water Res 41, 2871–2878.

[4] E. De Laurentiis, C. Prasse, T.A. Ternes, M. Minella, V. Maurino, C. Minero, M. Sarakha, M. Brigante, D. Vione, 2014. Assessing the photochemical transformation pathways of acetaminophen relevant to surface waters: Transformation kinetics, intermediates, and modelling, Water Res 53, 235–248.

[5] E. De Laurentiis, S. Chiron, S. Kouras-Hadef, C. Richard, M. Minella, V. Maurino, C. Minero, D. Vione, 2012. Photochemical fate of carbamazepine in surface freshwaters: Laboratory measures and modeling, Environ Sci Technol 46, 8164–8173.

[6] Q. Yin, Y. Ji, Y. Guo, K. Manoli, W. Chen, L. Zhang, X. Yu, M. Feng, 2024. Environmental fate and risk evolution of calcium channel blockers from chlorine-based disinfection to sunlit surface waters, Water Res 249, 120968.

[7] I. Loeff, A. Trelnln, H. Linschltz, 1983. Photochemistry of 9,10-Anthraquinone-2-sulfonate in Solution. 1. Intermediates and Mechanism, J. Phys. Chem. 87, 2536–2544.

[8] M. Bodrato, D. Vione, 2014. APEX (Aqueous Photochemistry of Environmentally occurring Xenobiotics): A free software tool to predict the kinetics of photochemical processes in surface waters, ENVIRON SCI-PROC IMP 16, 732–740.